Structure and composition of *Unio pictorum* shell: arguments for the diversity of the nacroprismatic arrangement in molluscs

Y. DAUPHIN*,† (iD), G. LUQUET‡, M. SALOME§, L. BELLOT-GURLET‖ (iD) & J.P. CUIF#

*Institut de Systématique, Evolution, Biodiversité, UMR 7205 CNRS MNHN UPMC EPHE Muséum National d'Histoire Naturelle, Paris, France

†Department of Biomaterials, Max-Planck-Institute of Colloids and Interfaces, Potsdam, Germany

‡Biologie des Organismes et Ecosystèmes Aquatiques, UMR 7208 CNRS MNHN UPMC UA UC IRD 207, Sorbonne Universités, Muséum National d'Histoire Naturelle, Paris, France

§ID21, European Synchrotron Radiation Facility, Grenoble, Cedex 9, France

‖De la Molécule aux Nano-Objets: Réactivité, Interactions et Spectroscopies, UMR 8233, UPMC CNRS Sorbonne Universités, Paris, France

#CR2P, Centre de Recherche sur la Paléodiversité et les Paléoenvironnements, UMR 7207, MNHN CNRS, Paris, France

Summary

Mollusc shells are complex organomineral structures, the arrangement and composition depending on the species. Most studies are dedicated to shells composed of an aragonite nacreous and a calcite prismatic layer, so the nacreous prismatic model based on *Pinctada* and *Atrina–Pinna*. Here, we studied the micro- and nanostructure, the mineralogy and composition of a nacroprismatic bivalve species: *Unio pictorum*. The prismatic layer of *Unio* is aragonite, and the inner structure of the prismatic units strongly differs from those of the calcitic layers. The shape of the prisms varies depending on their growth stage. The first layers of nacre are similar to those of gastropods (columnar nacre), then evolve towards the typical bivalve arrangement (sheet nacre). Na, Sr, Mg, P and S are present in both prisms and nacre. The organic prismatic envelopes are rich in sulphur amino acids, whereas organic sulphate is present within the prisms and the nacreous tablets. P is present as phosphate, probably a mixture of organic and mineral complex. Chemical distribution maps confirm the absence of an organic membrane between the nacre and the prisms. The comparison of the structure, mineralogy and composition of *Unio pictorum* and different species show the diversity of nacroprismatic shells, and that these features are taxonomically dependent.

Introduction

Calcareous biominerals are known in a large range of organisms, from Bacteria to eggshells. They are mainly calcite and/or

Correspondence to: Y. Dauphin, Institut de systématique, Evolution, Biodiversité, UMR 7205 CNRS MNHN UPMC EPHE Muséum National d'Histoire Naturelle, 55 Rue Buffon, F-75005 Paris, France. Tel: (33) 1 40 79 30 85; e-mail: yannicke. dauphin@upmc.fr; yannicke.dauphin@mpikg.mpg.de

aragonite, but vaterite and amorphous CaCO$_3$ are found. Although they are crystalline, calcareous biominerals exhibit unexpected characteristics in both structure and composition: they never display angles or facets. Their elemental chemical composition differs from that of their nonbiogenic counterparts, and is specific for the structure and the taxonomy. They sometimes show geometrical shape, but are surrounded by organic envelopes and contain intracrystalline organic matrices. All these features and paradoxes demonstrate that the deposition of calcareous biominerals is controlled by the organisms.

Coral skeletons and mollusc shells are the most studied, notably because they are (palaeo)environmental recorders. Most studies are dedicated to the mineral components (trace elements or isotopic ratios), but the ability to obtain *in situ* data at a microscale is now applicable to organic components. Thus, microstructures and composition can be associated to help to understand the biomineralisation processes. Elemental qualitative (maps) or quantitative chemical analyses are usually done using electron microprobe spectrometry. The differences between calcite and aragonite layers within a shell are evidenced. Organic envelopes surrounding the structural units such as prisms or tablets are visible in distribution maps, and their composition differs from that of the internal part of the structural unit. When the structural units are large, the maps reveal the heterogeneous distribution of chemical elements: growth layers are both structural and chemical. Up-to-now, most studied mollusc shells have a simple structure (nacre–prism), with large units and are bimineralogical (aragonite and calcite). Using such shells, it is possible to show that physiological changes occur during the growth. Despite what is commonly described, the growth of the calcitic prisms is not stopped by the nacre: the final part of the prisms has a special chemical composition (Dauphin *et al.*, 2008; Farre

et al., 2011; Cuif *et al.*, 2014). Moreover, the first mineral deposit on the organic terminal envelope of the prism is not nacre, but a fibrous aragonite. The presence of an organic layer between calcite and aragonite layers is also visible in the shells of other species of Pteriomorphia (Dauphin *et al.*, 2012, 2013).

The nacroprismatic arrangement is not so simple. Despite a morphological and mineralogical similarity, *Pinna* or *Atrina* and *Pinctada* differ although they are Pteriomorphia: the prisms of *Pinna nobilis* and *Atrina rigida* are monocrystalline, whereas the juvenile prisms of *Pinctada margaritifera* are monocrystalline, and the adult prisms are polycrystalline (Wada, 1956; Watabe & Wada, 1956; Dauphin, 2003). In other taxa, not only the nacre is aragonite, but the prismatic layer is (Boggild, 1930; Talylor *et al.*, 1969). In *Neotrigonia*, the two layers are not separated by an organic membrane, but prisms are separated by a thick organic envelope, and their inner structure is complex (Checa *et al.*, 2014; Dauphin *et al.*, 2014). Another example of the aragonitic nacroprismatic shell is that of *Unio pictorum*, a freshwater bivalve.

Unionidae have a worldwide distribution. They are sedentary filter feeders so that they are often used as environmental recorder for polluted environments (Cassini *et al.*, 1986; Balogh, 1988; Kurunczi *et al.*, 2001; Al-Bassam, 2005; Ravera *et al.*, 2003, 2007) or proxies for seasonal climate changes (Versteegh *et al.*, 2009, 2010). They are one of the most endangered groups: in the United States, nearly 70 species are either endangered or threatened (USFWS, 2003). From a geological point of view, Unionidae are known since the Triassic (Watters, 2001; Bogan & Roe, 2008) and are used to reconstruct palaeoenvironments (Schöll-Barna *et al.*, 2012; Findlater *et al.*, 2014).

Archaeological and fossil specimens are submitted to diagenetic changes, and these changes must be detected to obtain reliable reconstructions. Dramatic diagenesis modifies the structure and/or the mineralogy, but some aragonite–calcite changes have been observed without microstructural modifications (Dauphin, 1986; Dauphin & Denis, 1990; Hikida *et al.*, 1993). To detect minor diagenetic alterations, the structure and composition of modern samples must be deciphered at a micro- and nanoscale. Because *Unio* shells are said to be classically nacroprismatic, little attention has been paid to their structure (Taylor *et al.*, 1969; Checa & Rodriguez-Navarro, 2001). Mollusc shells are not pure minerals, and studies are mainly focussed on proteins extracted from the nacreous layer of *Unio pictorum* (Marie *et al.*, 2007, 2008, 2010; Ramos-Silva *et al.*, 2012). Details about the prismatic layer are sparse (Marie *et al.*, 2007, 2008) and the relationships between the structure and the molecular composition are not well known.

In this paper, we re-examine in detail the microstructure and nanostructure of the shell of *Unio pictorum*. We investigate the nanostructure of the nacre and prisms, their mineralogy and the topographical relationships between the structure and the

chemical composition. A comparison with other nacroprismatic arrangements is done.

Material and methods

Materials

Mussels of the genus *Unio* are freshwater bivalve molluscs. Several species are present in European rivers and lakes. Among them, *Unio pictorum* (Linnaeus, 1758) is commonly called the 'thick shelled painter's mussel'. They can reach an age of about 15 years. The yellow to green shell is flat, equivalve, inequilateral with an oval outline (Fig. 1). The inner view shows the hinge with teeth, muscle scars and the pallial line, whereas the ligament is external. Three shells have been used for SEM, AFM and EDS studies, two shells have been used for XANES analyses.

Light microscopy

Optical microscopy includes observation by transmitted light (natural and crossed Nicols polarisation) on ultrathin sections perpendicular to the surface of the shells, and reflected natural light on polished surfaces.

Scanning electron microscope (SEM)

Surfaces and sections (cut perpendicular to the surface of the shells) were prepared. Polished sections and some fractures were etched to reveal microstructural features. The detailed procedures of the sample preparations are given in the figure legends. Scanning electron microscope (SEM) observations were conducted using a Philips 505, a Philips XL30 (Philips, Eindhoven, the Netherlands) and a JEOL JCM6000 (JEOL ltd, Tolyo, Japan) instrument in secondary electron mode on Au–Pd coated samples. Uncoated preparations were observed
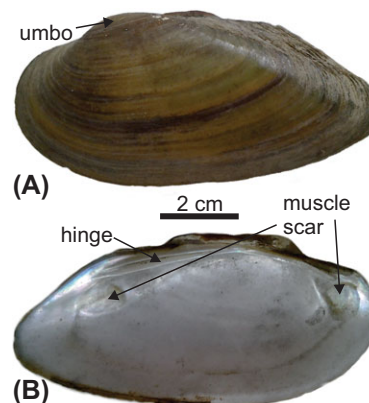

Fig. 1. Morphology of *Unio pictorum* (left valve). (A) Outer surface showing growth layers and a partly preserved periostracum. (B) Inner view of the same valve, the main part being nacre.

using a Phenom ProX and a FEI FESEM Quanta F600 in backscattered electron mode (BSE).

Atomic force microscope (AFM)

The atomic force microscope (AFM) maps the surface topography of the sample. The resolution of tapping mode AFM is in the order of a few nm. Tip - sample force interactions cause changes in amplitude, phase and the resonance frequency of the oscillating cantilever. The spatial variation of the change can be presented in height (topography) or interaction (amplitude or phase) images that are collected simultaneously. Phase images can be generated as a consequence of variations in material properties including composition, friction and adhesion. It is generally admitted that hard materials have a light aspect in AFM, so that the darker regions correspond to soft material, organic matter or amorphous minerals (Haugstad, 2012; Mittal & Matsko, 2012).

AFM observations were conducted in air at room temperature using a Nanoscope IIIa Dimension 3100 (Bruker, Germany). The probe consists of a cantilever with an integrated silicon nitride tip. Micron scale images were acquired using the tapping mode. The detailed procedures of the sample preparations are given in the figure captions.

Raman spectroscopy

Raman analyses were done using a Senterra Raman microspectrometer (Bruker Optics), using a laser emitting at 785 nm settled to provide a laser power at the sample of about 15 mW. Data collection was controlled by the OPUS 7.5 software (Bruker Optics). Measurements were collected across one spectral window ($100-1540$ cm^{-1}) at a spectral resolution of about 3 cm^{-1}, and each analysis was the coaddition of 2 spectra accumulated at up to 100 s exposures each. Analyses were performed using a $100\times$ IR objective (Olympus, Tokyo, Japan), giving an analytical spot size of approximately 2 μm diameter with the used excitation length. Analyses were directly performed on polished surfaces across the thickness of the shells. A fluorescence background was removed for the mamelon spectra only.

Elemental analysis by EDS (energy dispersive X-ray spectroscopy)

Samples were embedded in resin and polished with diamond pastes. The analysis positions were chosen to reflect known structural features in the cross section of the shell. Measurements were made on carbon-coated samples. EDS was undertaken using a PHENOM PRO X with the EID software. Operating conditions for elemental distribution maps were 15 kV accelerating voltage, a dwell time of 250 ms, and a 256 pixels resolution.

Micro-XANES – X-ray absorption near edge structure spectroscopy

This work was carried out at the ID21 beamline of the European Synchrotron Radiation Facility during two different experimental sessions. The ID21 scanning X-ray microscope uses Fresnel zone plates or Kirkpatrick–Baez mirrors as focussing optics to generate a submicron X-ray probe. An energy-dispersive fluorescence detector mounted in the horizontal plane collects the fluorescence emission photons. An energy range between 2 and 7 keV is available, which gives access to the K-edge of sulphur at 2472 eV and to the K-edge of phosphorus at 2145 eV. The XANES energy scan around the sulphur or phosphorus K-edge is achieved using a fixed-exit double-crystal Si(111) monochromator located upstream from the microscope, which offers the necessary energy resolution. This experiment required the X-ray microscope to be operated under vacuum to avoid the strong absorption of the sulphur and phosphorus emission lines by air. Although the primary beam energy was set around that of the S or P K-edge energy region, elements with absorption edges at lower energies were also subject to excitation and emission of fluorescence photons, and could therefore be determined.

During the first experimental session (proposal EC-545) in 2010, a zone plate (ZonePLate Ltd, UK) achieving a microbeam spot size of 0.2×0.7 μm^2 (V $\times$ H) with 2.5×10^9 photons s^{-1} was used. The fluorescence detector was a 30 mm^2 high-purity Ge detector (Princeton Gamma-Tech, USA). During the second experimental session (proposal LS-2563) in 2016, a Kirkpatrick–Baez mirror system focussed the beam to a 0.5×0.6 μm^2 (V $\times$ H) spot with 4×10^9 photons s^{-1}. The fluorescence detector was a 80 mm^2 Silicon Drift Diode (Bruker).

X-ray microfluorescence (XRF) element maps of Mg, Na and Sr were obtained simultaneously with the S or P maps, so that possible correlations between element repartition will be visible. Polished samples were etched with 1% (v/v) acetic acid for 5 s. Etching of the sample after polishing helped to eliminate potential surface contamination and remains of the diamond pastes and oil.

Results

Both layers of the *Unio pictorum* shell are aragonite, but the thin outer layer is prismatic and the thick inner layer is nacreous (Fig. 2A).

Micro- and nanostructure

Viewed using cross-polarised light, the prisms are brilliantly and heterogeneously coloured, so they are not monocrystalline (Fig. 2B). The outer prismatic layer is covered by a thick periostracum (Fig. 2C: pe) and the prismatic units are separated by organic membranes (Fig. 2C: m). The initial parts
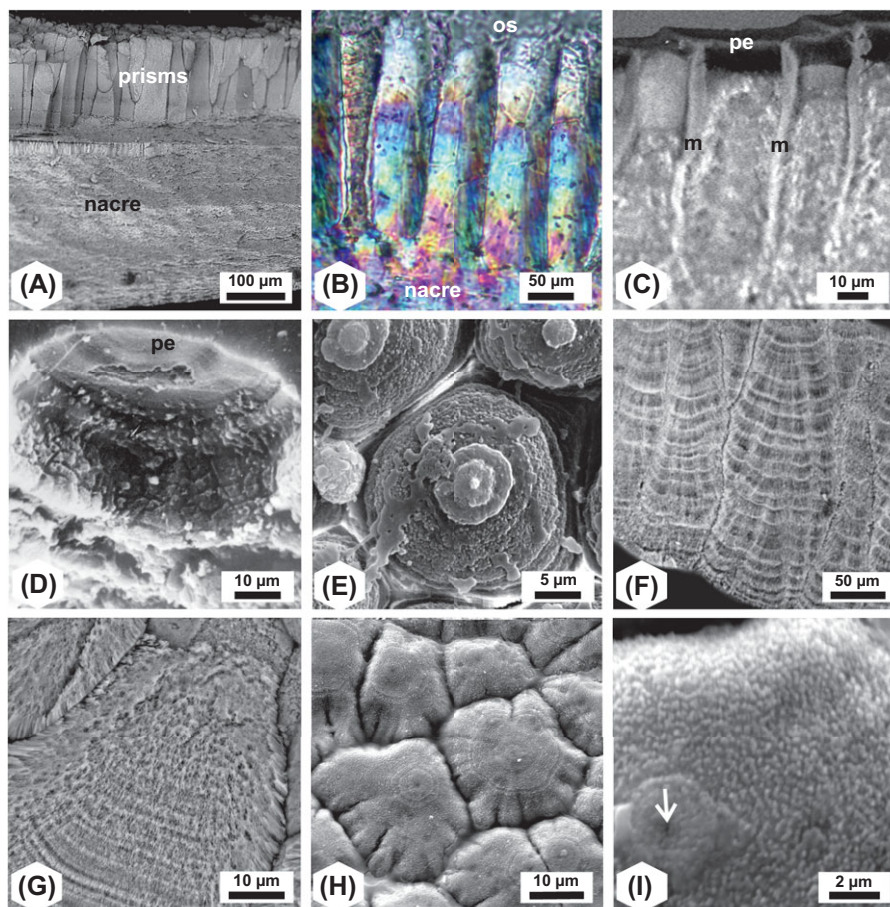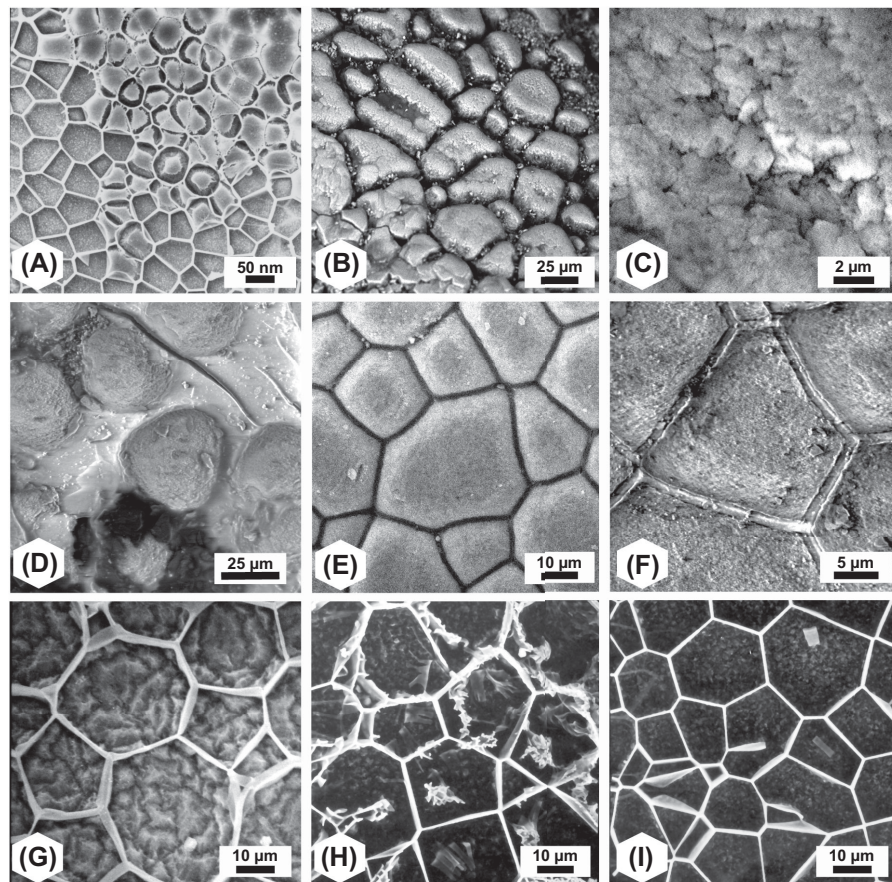
Fig. 2. Structure of the prismatic layer. (A) Vertical section showing the outer prismatic layer and the thick inner nacreous layer. (B) Thin section of the prismatic layer and the first layers of nacre, seen using cross polarised visible light microscopy. Different colours are visible in a single prism, showing it is not monocrystalline. (C) Vertical fracture showing remains of the periostracum (pe) and the organic membranes surrounding the prisms (m). (D) Detail of the initial mamelon with remains of the periostracum (pe). (E) Concentric growth layers at the first stages of the prisms. Fixed sample (glutaraldehyde 3%), then decalcified (RDO 25% for 30 s); remains of the organic matrix were partly destroyed (commercial NaClO for 1 h). (F) Vertical section showing the growth layers in the prisms and the divergent elongated crystallites. Etched using acetic acid 0.1% for 10 s. (G) Vertical unetched fracture showing the oblique elongated crystallites at the periphery of the prism, and growth layers. (H) Outer surface showing the complex shape of the prisms after removal of the periostracum using KOH 1 M for 19 h 30 min at room temperature. Circular growth lines are visible. (I) Detail of the central part of a prism, showing a granular structure and a central hole (arrow).

of the prisms are small, not contiguous, with a prominent knob or mamelon, here covered by remains of the periostracum (Figs. 2C, D: pe). The concentric layered structure of the mamelons is visible after the removal of the periostracum (Fig. 2E). The diameter of the prisms can reach 80 μm, their length is about 150–200 μm. Polished and etched surfaces reveal the presence of minor and major curved growth layers (Fig. 2F). Growth layers are synchronous across adjacent prisms. Divergent acicular crystallites are visible within the prisms (Fig. 2G). The shape of the prisms is variable across the thickness of the shell. The initial zone is more or less round, but the outer part has a complex outline with lobes (Fig. 2H). The surface of these prisms is 'granular', the granules being the extremities of the acicular crystallites (Fig. 2I).

Fixed and etched surfaces, a few micrometres under the periostracum, show the organic membranes surrounding the prisms (Fig. 3A). Prisms of the inner surface in the growing zone differ from those of the outer surface. A fixed and etched fracture shows that the size and shape are irregular, and the prismatic units are separated by a thick organic envelope (Fig. 3B). The surface is divided into smaller irregular units (Fig. 3C). At the growing edge of the shell, prisms are still embedded in the organic matrix and they are not contiguous (Fig. 3D). They are more or less polygonal between the nacreous layer and the outer edge of the shell (Figs. 3E, F). In polished and transverse sections, the complex inner structure is visible (Fig. 3G), as well as the organic membranes (Figs. 3G–I). Inner membranes corresponding to the lobes are sometimes visible (Fig. 3H).

Fig. 3. Structure of the prismatic layer (SEM images). (A) Transverse section near the outer surface of the shell showing the organic envelopes of the prisms and remains of the periostracum. Fixation (glutaraldehyde 3%), then decalcification in a 12.5% solution of RDO (Rapid Bone Decalcifier) for 30 s. (B) Inner surface near the growing edge of the valve; unetched sample. (C) Detail of Figure 3(B), showing the complex inner structure of a prism. (D) First stage of prisms still embedded in an organic matrix at the external part of the growing edge. (E), (F) Inner surfaces showing polygonal prisms surrounded by a thick organic envelope. (G) Polished and etched section showing the organic envelopes and the inner structure of the prismatic units. Fixation (glutaraldehyde 3%), then decalcification (RDO 25% for 30 s). (H) Polished and etched section showing the polygonal shape of the prisms, the envelopes and inner organic membranes. Fixation (glutaraldehyde 3%), then decalcification (RDO 12.5% for 30 s). (I) Same polished and etched section showing the polygonal shape of the prisms and the envelopes.

The central part of the prisms and the granular arrangement of the outer surface observed using AFM height images are similar to SEM images (Figs. 4A, B). The acicular crystallites seen with SEM are composed of rounded nanogranules (Figs. 4C, D). In phase images, the colour of a granule is not uniform, so that the composition is heterogeneous (Fig. 4E). Strongly etched and fixed sections show the organic matrix network within a prism (Fig. 4F).

The nacreous layer is thick, with regular tablets. The first layers do not form a step-like pattern in surface or lens in vertical sections, said to be characteristic for Bivalvia. They look like the columnar arrangement described in gastropods (Figs. 5A, B). Little by little, the arrangement becomes similar to that of the Bivalves and the inner surface of the shell shows the regular step pattern (Fig. 5C). Tablets are not contiguous and more or less circular before to be adjacent (Fig. 5D). The

inner structure of the nacreous layer shows the irregular granules, without facets (Fig. 5E). These granules are surrounded by a cortex (Fig. 5F).

Growth lines are visible at the end of the prismatic layer in ultrathin sections (Fig. 6A). Fractures show the absence of an organic membrane between nacre and prisms and the boundary between the two layers is wavy and not sharp (Figs. 6B–F). Observations of the inner surface near the growing zone confirm the absence of an organic membrane between nacre and prisms (Figs. 6G, H), but the interprismatic membrane is present, whatever the regularity of the prisms (Fig. 6I).

Mineralogy

Raman spectra (Fig. 7A) show that the two layers are aragonite, with a sharp peak at 1085 cm^{-1} for CO_3^{2-}
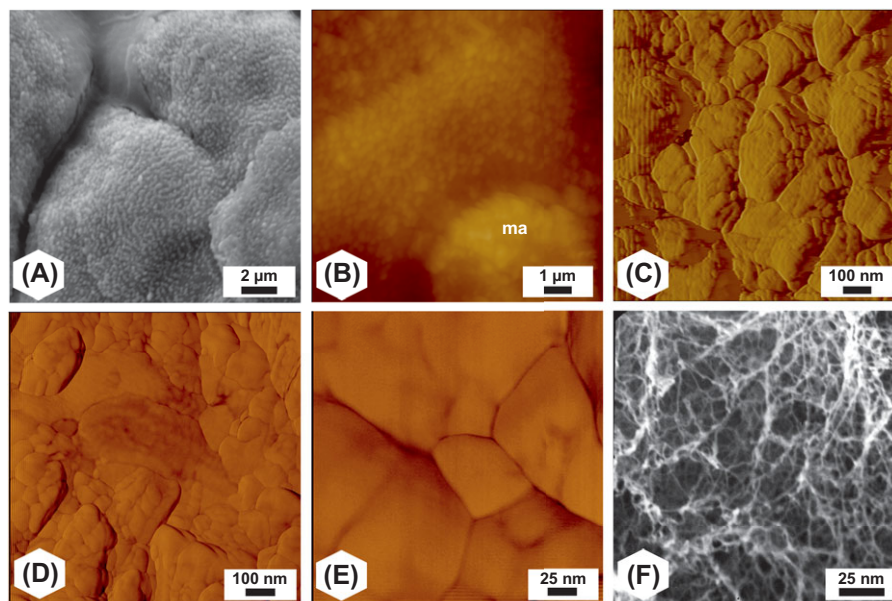
Fig. 4. Nanostructures of the prismatic layer. (A) Outer surface of a prism showing the granular structure; periostracum destroyed using KOH 1 M for 19 h 30 min at room temperature; SEM image. (B)–(E) Same zone, showing that every granule is composed of several smaller rounded units; AFM phase images. (F) SEM image of the intraprismatic organic network visible after fixation (glutaraldehyde 3%) and decalcification (RDO 25% for 30 s). ma: mamelon.
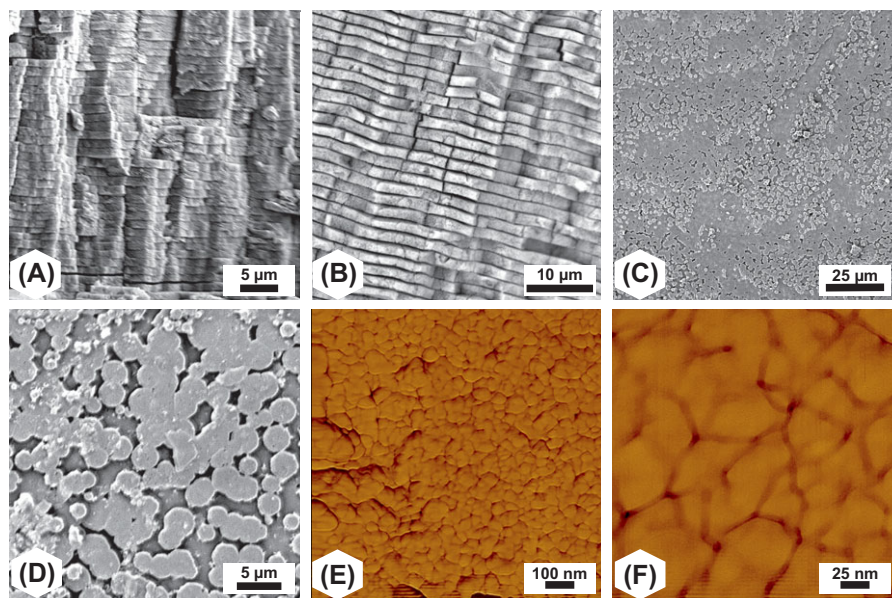
Fig. 5. Nacreous layer. (A) Columnar arrangement of the outer part (near the prisms) of the layer; unetched sample. (B) Detail of the same sample showing the regular thickness of the tablets. (C) Inner surface of the valve showing the step structure, corresponding to a lenticular arrangement in vertical section; cleaned using KOH 1 M for 45 min. (D) Same sample: inner surface showing round immature tablets. (E), (F) AFM phase images showing the granular structure of the tablets; unetched surfaces.

symmetric stretching (ν_1 mode) and a doublet at 702 and 706 cm^{-1} for the in-plane bending (ν_4 mode). Nevertheless, some differences are visible. The mamelon raw spectrum (data not shown) exhibits a moderate fluorescence due to the organic matrix and remains of the periostracum. On the con-

trary, there is no fluorescence contribution to the prisms and nacre spectra. The values of the full width at half maximum (FWHM) for the ν_1 and ν_4 bands representative of the three layers are similar (Fig. 7B). The spectra relative intensities and shapes underline that the crystallinity of the aragonite in
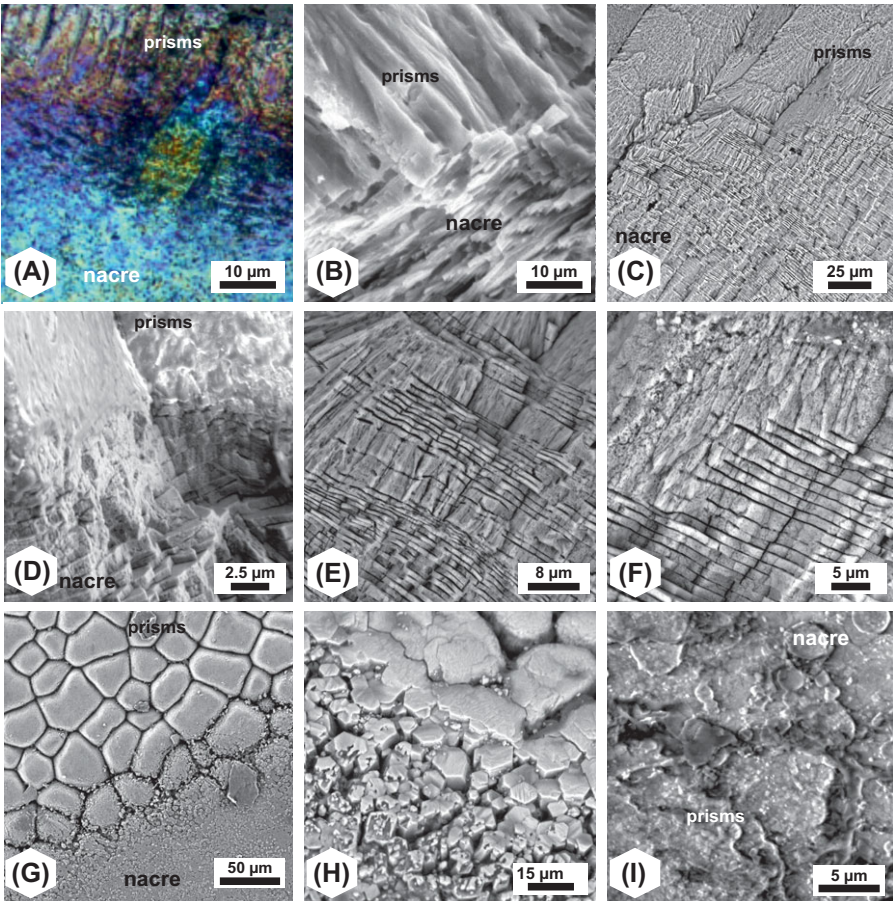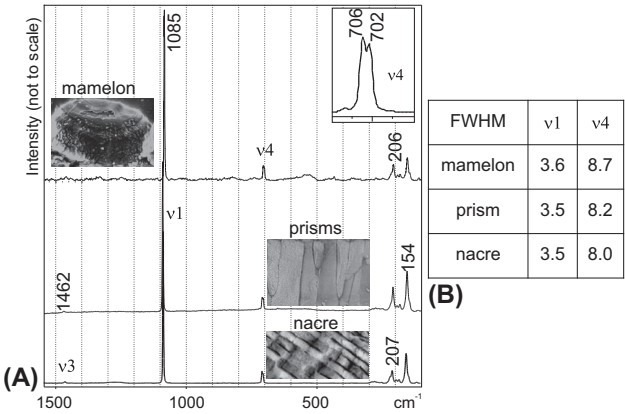
Fig. 6. Prisms–nacre transition. (A) Thin section seen using cross polarised visible light microscopy, showing growth lines at the end of the prisms and the absence of a sharp boundary between the two layers. (B) Fracture showing the irregular transition between nacre and prisms, and the absence of an organic membrane. (C) Vertical unetched fracture showing that the shape of the growth lines is modified from the prisms to the nacre. No organic layer is visible. (D) Unetched vertical fracture showing the end of a prism and the first tablets. (E), (F) Unetched vertical fracture showing the irregularity of the layered structure. (G)–(I) Inner surface of a valve showing the large prisms and the first layers of nacre.

Fig. 7. Raman spectra of the outer mamelon, prisms and nacre, showing they are aragonite.

the mamelon slightly differs from that of the prism. No amorphous $CaCO_3$ was detected over the several measurements performed, likewise no peaks indicative of PO_4 were noticed.

Chemical composition

SEM-EDS qualitative distribution maps were acquired from the end of the prisms to the beginning of the nacreous layer (Fig. S1A). Organic membranes between two prisms were included. Ca, C and the usual chemical minor elements detected in mollusc shells are present (Na, Mg, P, Cl and Sr) in low quantities. Distribution maps show that the 'black' interprismatic membranes seen in BSE images are poor in Ca (Fig. S1B). No distinct boundary, no distinct membranes between the prisms and the nacre are displayed in the distribution maps in the two studies zones (Figs. S1C–H). The interprismatic organic membrane is sometimes faint, but the regular layered arrangement in the nacre becomes more visible towards the inner part of the layer.
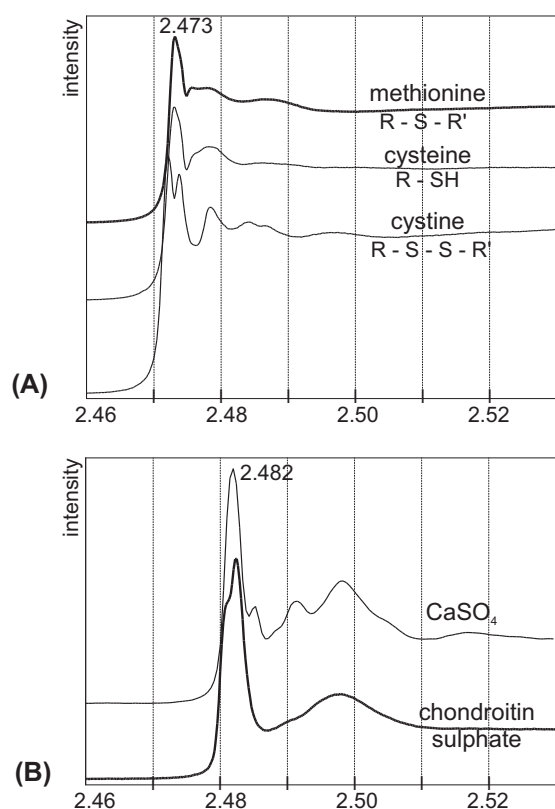
Fig. 8. XANES spectra at the S K-edge for S containing standards. (A) S amino acids showing a main peak at 2.473 keV. (B) Sulphated standards: chondroitin sulphate (organic) and CaSO₄ (mineral) showing a main peak at 2.482 keV.

Figure S2 shows the chemical elements detected when the set-up is established for the XANES analyses at the S K-edge. Na and Sr are usually present in aragonite molluscan layers, as well as Mg, P and S. These results are consistent with those of EDS.

Organic and inorganic standards have been used for XANES at the P and S K-edge. The peak of sulphur present in amino acids is at 2.473 keV (Fig. 8A), whereas the peak for sulphated components is at 2.482 keV (Fig. 8B). The broad secondary peak around 2.50 keV is rather smooth for the organic sample and subdivided for the mineral sample. The main peak for the P containing standards is at about 2.15 keV (Fig. 9). In all samples, P is associated to phosphate groups, except for elemental P. The mineral Ca–P association is linked with the appearance of a peak shoulder near 2.155 keV. Such a peak is absent in organic components. Again, mineral and organic samples differ in the second part of the spectra: rather smooth for the organic samples, several broad peaks are present in the mineral components. The main peak of elemental P is at 2.145 keV (Fig. 9), and the second part of the spectrum clearly differs from that of PO_4 components.

The *in situ* XANES spectra performed on a polished surface of the *Unio pictorum* shell is noisy, the P content being low (about
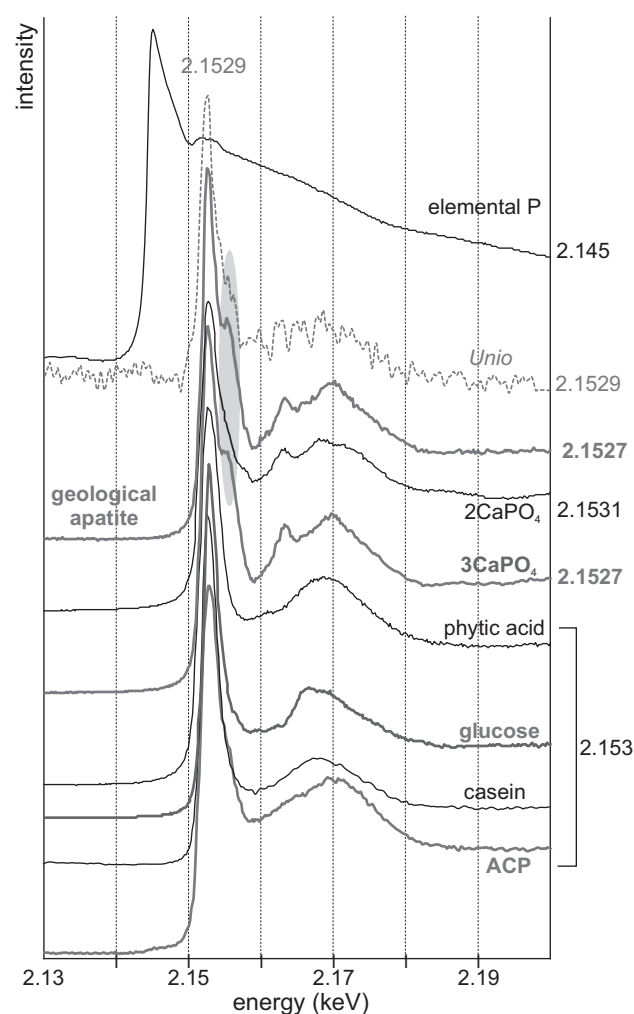

Fig. 9. XANES spectra at the P K-edge for standard phosphorylated samples, elemental P and *Unio pictorum* shell. ACP: amorphous Ca phosphate mineral; organic samples: casein, glucose 6-P, phytic acid; mineral samples: tricalcium phosphate ($Ca_3(PO_4)_2$), dibasic calcium phosphate ($CaHPO_4$), geological apatite; organomineral sample: *Unio* pictorum shell.

Table 1. Linear correlation coefficient between the spectra of *Unio pictorum* and standards.

Casein	0.89
Phytic acid	0.86
Glucose 6P	0.83
ACP	0.78
3CaPO₄	0.76
2CaPO₄	0.68
Geol. apatite	0.81

500 ppm). The main peak is at 2.153 keV (Fig. 9), indicative of PO_4. A weak shoulder is also visible, suggesting that Ca and P are associated in the shell. The correlation coefficient between *U. pictorum* and the casein is $r = 0.89$ and $r = 0.81$ for *U. pictorum* versus geological apatite (Table 1).
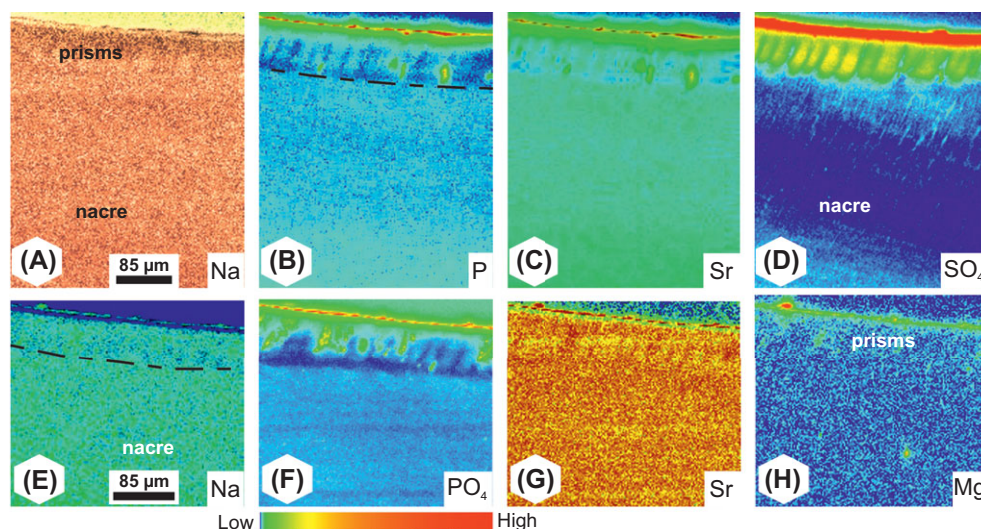
Fig. 10. (A)–(C) XRF maps for Na, P and Sr on a vertical section of the shell of *Unio pictorum* showing the thin outer prismatic layer, and a part of the thick inner nacreous layer. (D) XRF distribution map of the sulphated components. (E), (G)–(H) XRF elemental maps for Na, Sr and Mg at another location. (F) XRF distribution maps of the phosphated components.

The spatial distribution of S was obtained by micro-X-Ray Fluorescence mapping on a vertical section across the nacreous and prismatic layers (Figs. 10, 11). The spatial distribution of fluorescing elements such as Mg, Na was also obtained. Na, Mg and Sr contents are similar in both layers, but the boundaries of the prisms are visible in the outer layer, whereas the nacreous layer does not display a distinct structure (Figs. 10, 11). There are no sharp limits between the two layers. Differences are stronger for P and S. The elemental P content of the nacre is higher than that of the prisms (Fig. 10B), especially towards the inner surface of the shell (Fig. 10B). The difference in Sr is faint, both layers being aragonite (Fig. 10C). The XANES map performed at 2.482 keV shows that the prisms are rich and the nacre is poor in sulphated components (Fig. 10D). The nacreous layer is heterogeneous and shows an inner 'columnar' structure reminiscent of what has been observed in SEM images. As for P, there is a gradient between the inner and outer parts of the nacre. The XANES map done at the energy of PO_4 confirms the lower content of the nacreous layer and of the end of the prismatic layer (Fig. 10F). The outer part of the prismatic layer, adjacent to the periostracum, has the highest PO_4 content. The inner parts of the prisms are richer than the organic membranes (Fig. 10F).

More detailed XRF maps have been dedicated to the transition between the prisms and the nacre, and to the structure of the prisms (Fig. 11). The Sr content of the prismatic layer is slightly higher than that of the nacre (Fig. 11A). The X-Ray Fluorescence map of the sulphur associated to amino acids reveals the high S content of the interprismatic membranes (Fig. 11B). The layered pattern of the nacreous layer is visible in the sulphate map (Fig. 11C). The interprismatic organic envelopes are visible in all XRF maps (Figs. 11B–F), and a faint growth pattern is displayed in the sulphate map (Fig. 11F).

Discussion

Structures and mineralogy

The nacroprismatic arrangement is the most studied among mollusc shells although it is rare. Usually, the 'model' is *Atrina rigida* or *Pinctada sp.* in which the prismatic layer is calcite and separated from the aragonitic nacre by an organic layer.

The three layered shell of *Unio sp.*: an outer thick periostracum, a prismatic layer and a thick nacreous layer, as well as the aragonite mineralogy, have been described by Schmidt (1924).

The prismatic layer of *Unio pictorum* is aragonite, but this difference with the calcite prisms of *Atrina* and *Pinctada* is not the only one. In the *Unio* shell, nacre and prisms are not separated by an organic layer. A similar feature was previously observed in *Neotrigonia sp.* (Dauphin *et al.*, 2014). The transition between the two layers is smooth, and clearly different from what is known in Pteriomorphia.

The usual arrangement of the nacreous layer of bivalve shell is the lenticular type, whereas the columnar type is said to be characteristic of gastropods and cephalopods (Wise, 1970). Nevertheless, the nacreous tablets adjacent to the prismatic layer show a columnar arrangement. Then the lenticular type is developed. Two arrangements of the nacreous tablets have been described by Taylor *et al.* (1969) in several species of Unionidae. Again, a similar feature was described in the *Neotrigonia* shell (Dauphin *et al.*, 2014).

The prismatic units of *U. pictorum* are separated by thick organic envelopes, and the sections parallel to the long axis show growth layers, as for *Pinna nobilis* or *Pinctada sp.* (Taylor *et al.*, 1969). Grégoire (1961) has observed that in Unionid shells, an aragonite prism is an aggregate of small crystals.
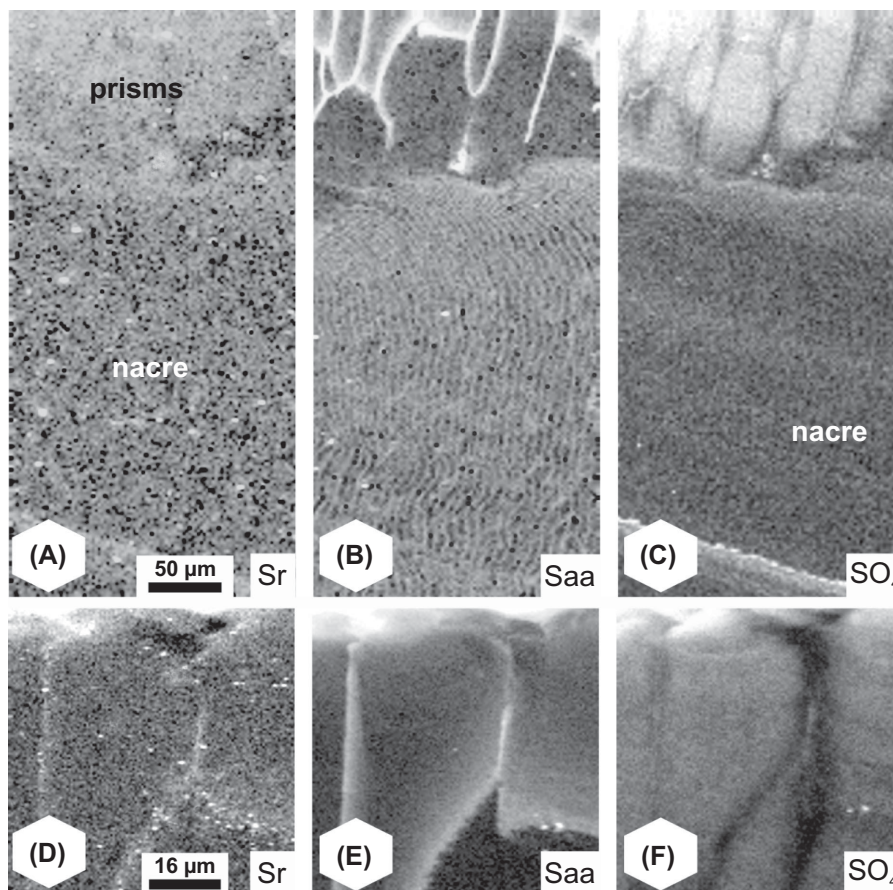
Fig. 11. Detailed XRF maps showing the prism–nacre transition (A–C), and the prismatic units (D–F). S amino acids map (Saa) shows the high content of the organic envelopes surrounding the prisms.

Nevertheless, prisms are described as 'aragonite simple prisms' and show 'a typical feathery appearance, due to diverging longitudinal striations' (Taylor *et al.*, 1969). Maybe the most striking characteristic of the prisms of *Unio* is the 'plasticity' of their shape during their growth. Such a feature is not described in *Neotrigonia*, and the polygonal shape of the calcitic prismatic units of Pteriomorphia is regular. The prismatic units of *U. pictorum* are often curved, and their inner structure is more complex than that described by Taylor *et al.* (1969), so that the inorganic model of Grigor'ev (1965) is not appropriate to explain the growth of the prisms of *Unio*.

Thus, the transition between nacre and prisms, the shape and inner structure of the prisms as well as the arrangement of the first nacreous layers clearly differ from those of the *Pinna–Pinctada* 'nacroprismatic model'.

Structure and composition

Quantitative analysis of S and P contents of the shells of *Unio* are rare. Vinogradov (1953) has collected chemical data on marine organisms, but some data on freshwater shells are given. For *Unio crassum and U. pictorum,* SO_4 content varies from 0.08% to 1.85%. This discrepancy probably depends on the presence or absence of the periostracum. Only one analysis is provided for P_2O_5: 0.16%, that is a P content of 682 ppm. This is consistent with the data of Krolak & Zdanowski (2007) indicating an amount of P ranging from 450 to 620 ppm. This low amount of P content accounts for the absence of PO_4 vibrational signature on the recorded Raman spectra, besides with the intense carbonate signature, which dominates the spectra.

Distribution maps show that despite a common mineralogy (aragonite), the elemental composition of nacre and prisms differs. Moreover, the nacre is not homogeneous in P and S contents. Detailed X-Ray Fluorescence maps clearly show the prismatic units and their envelopes. These envelopes are rich in both P and S. Although the envelopes are rich in S amino acids, the inner part of the prisms is rich in S as organic sulphate. In all layers and transition, P is in PO_4 complex.

Are S and P organic or mineral?

Despite most studies of mollusc shell composition are dedicated to Mg and Sr, S is present in the data of Clarke & Wheeler

(1922). The high S content of the periostracum + outer layer of bivalve shells has been evidenced by Horiguchi (1959). This author also shows the presence of S as organic sulphate in the shells. Enzymatic hydrolyses and stained sections have shown that the small crystals of the regenerating shell of a gastropod are rich in acidic and sulphated polysaccharides (Abolins-Krogis, 1958). Wada (1964) and Wada & Furuhashi (1970) have found an acidic mucopolysaccharide similar to chondroitin sulphate in the shell of several bivalve species. Simkiss (1965) has confirmed that the organic matrix extracted from the shell of an oyster contains a sulphated polysaccharide, the infrared spectra being similar to that of chondroitin sulphate. Sulphates were detected in the central part of the nacreous tablets of cephalopods, but not in bivalves (Crenshaw & Ristedt, 1976; Nudelman *et al.*, 2006). Electrophoretic and XANES analyses of the organic matrices of several species of mollusc shells have confirmed the presence of acidic sulphated mucopolysaccharides, and distribution maps have shown the relationships between the structure and composition (Cuif *et al.*, 2003; Dauphin *et al.*, 2003). Moreover, XANES maps have displayed the differences between the organic envelopes surrounding the microstructural units and the inner part of these units, as well as the presence of sulphur amino acids in the insoluble matrices. The sugar moieties of the 95, 50 and 29 kDa glycoproteins in the soluble organic matrix of the nacreous layer of *U. pictorum* are acidic and sulphated (Marie *et al.*, 2007, 2010). So, it can be suggested that the sulphated components of the nacreous and prismatic layers of *U. pictorum* shell, displayed in the XANES maps, are acidic sulphated sugars.

Phosphorus was detected in the insoluble organic matrix of some bivalve shells with different microstructural arrangements (Horiguchi, 1959). Most studies dedicated to phosphoproteins are based on bone. Phosphorylated proteins have been detected in the soluble matrix of the calcitic shell of *Crassostrea virginica* (Sikes & Wheeler, 1983; Bordas *et al.*, 1991; Wheeler, 1992; Johnstone, 2008), and PO_4 represent about 15% by weight (Rusenko, 1988). Phosphorylated proteins have been detected in the calcitic shell of *Patinopecten yessoensis* (Sarashina & Endo, 2001). PO_4 content of the dry soluble matrix of calcitic layers is higher than that of aragonitic layers, and varies from 0.26% (*Mercenaria mercenaria*) to 22.4% (*Placopecten maximus*) (Bordas *et al.*, 1991; Johnstone, 2008). Phosphoproteins are also known in the soluble organic matrix of the nacreous layer of *Pteria penguin* (Naganuma *et al.*, 2014). Bevelander (1952) using the ^{32}P radioisotope has shown its intake in the organic envelopes of the prisms of *Pinna*, envelopes he called periostracum: 'It seems fairly evident from our observations that the phosphorus in the shell is confined to the organic constituent of the exoskeletal complex'.

The comparison of the XANES spectra of standard samples and *Unio*, shows that the highest linear correlation coefficients are between the organic standards and *U. pictorum* (Table 1).

Nevertheless, the presence of mineral PO_4 cannot be excluded: the presence in P–XANES spectrum of a shoulder at energies slightly greater than the primary edge is characteristic of Ca–P association (Brandes *et al.*, 2007).

S and P roles in biomineralisation

Sulphur and organic sulphates are known in Mollusc shells in the granules deposited in repair processes, and they bind Ca to the mucopolysaccharides (Abolins-Krogis, 1958; Wada, 1964, 1980). Phosphates are known as intracellular minerals associated to Ca, Mg and CO_3 (Simkiss, 1976). Greenfield *et al.* (1984) have shown that the soluble organic matrix extracted from *Mercenaria* shells 'binds phosphate, but only in the presence of calcium'. *Mercenaria* and *Mytilus* shells contain sulphate, probably in the form of sulphated carbohydrates, but their soluble organic matrices are not phosphorylated (Wheeler, 1992). On the opposite, *Crassostrea* matrices contain phosphate. From the comparison of the microstructures of the shells and the composition of their organic matrices, Wheeler (1992) states that: 'Given that all-these species have different shell microstructures, the dichotomy of sulphated *versus* phosphorylated matrix raises the question of whether the type of anion found in matrix is an important factor in controlling the shell crystal architecture'.

Comparison with other nacroprismatic shells

Unio shells belong to the most studied type of Mollusc shell: nacroprismatic. This two-layered structure is variable: nacre is always aragonite, but prisms are either calcite or aragonite, depending on the taxonomy of the sample. The arrangement of the nacreous tablets (columnar, lens), the shape of the tablets (hexagonal, rectangular etc.), their inner structure etc. are species specific (Wise, 1970; Mutvei, 1977). The size, shape, density and inner structures of the prisms are also species dependent. The elemental composition of both nacre and prisms is species specific (Masuda & Hirano, 1980; Dauphin *et al.*, 1989). Previous analyses have also shown that the soluble organic matrices of the prisms of *Pinna* are rich in acidic sulphated sugars, whereas the prisms of *Pinctada* are rich in proteins, despite they are calcite (Dauphin, 2003; Dauphin *et al.*, 2003). Molecular weights, amino-acid composition and acidity also differ. In these shells, calcite and aragonite are clearly separated by a thick organic membrane. The chemical content of the end of the calcitic prisms is modified, and the first layer of aragonitic is fibrous (Dauphin *et al.*, 2003). The chemical composition of the fibrous aragonite is not that of the nacre (Farre *et al.*, 2011).

Aragonitic prisms are still poorly known. *Anodonta* belongs to the Unionidae family. The interface between the aragonitic prisms and the nacre has been described in two species (Freer *et al.*, 2010). Nevertheless, SEM images do not show the transition between the two structures. Images display the

interprismatic membranes, but not the membranes between prisms and nacre. Elemental distributions maps and XANES maps confirm the difference between the nacrocalcitic prismatic and nacroaragonitic prismatic arrangement in both *Neotrigonia* (Dauphin et al., 2014) and *Unio*. Whereas the boundary between nacre and prisms is visible in *Neotrigonia* at low magnifications, it is not so evident for *Unio*. Nevertheless, in both species, it is difficult to draw a line between the two layers using large magnifications, and there is no fibrous aragonite between nacre and prisms. Another difference is the structure of the aragonitic prisms: the outer face adjacent to the periostracum consists of distinct knobs. The inner structure of the aragonitic prisms differs from those of calcitic prisms, with a fascicular arrangement. Although they are both aragonite, the morphology, and the growth mode of the prisms of *Neotrigonia* and *Unio* also differ. The shape of the prisms of *Neotrigonia* is regular, whereas the prisms of *Unio* are complex (Schoeppler & Zlotnikov, 2017).

A nacroprismatic structure is also known in gastropods. Because of the complex helicoidal shells, these shells are not often described. Among them, *Turbo* and *Trochus* are most known for their beautiful and thick layer of nacre, and their thin aragonite prismatic layer is not well studied (Grégoire, 1961; McClintock, 1967). The last part of the shell of the abalone is almost flat, and so to do well oriented sections is easy. Moreover, the inner nacreous layer is highly irridescent with attractive colours. One hundred species are described in *Haliotis*, and the structural arrangement of the shell layers has been described in less than twenty species (Dauphin *et al.*, 1989; Mutvei *et al.*, 1985). In all species, the inner layer is the aragonite nacre, but the outer layer is prismatic. The outer layer is aragonite, or calcite, or calcite and aragonite (Mutvei *et al.*, 1985). Despite this variability between the different species, the structure is constant within a species. When calcite and aragonite are present in the outer layer, their respective abundance and distribution are species dependent. Elemental chemical analyses have shown that nacre and prisms, both aragonite, have different compositions (Dauphin *et al.*, 2013).

From these data, a unique and simple nacroprismatic arrangement does not exist; variability in the inner structure of prisms and nacre, their composition and the transition between the two layers are too diverse, despite a small number of shells has been studied from these points of view. The observed variability is not randomness, on the opposite, it is taxonomically dependent.

Conclusion

Variability in the microstructural arrangement and composition of Mollusc shells is known since the extensive work of Boggild (1930). A more detailed study on Bivalvia has confirmed that families and orders share common characteristics (Taylor *et al.*, 1969). Although more and more papers show that the microstructure, mineralogy and composition of shells are species dependent, these criteria are not yet used for taxonomic or phylogenetic purposes: diagnoses are mainly based on anatomy and morphology. Biologists are able to use the criteria of soft tissues and organs to establish precise diagnoses; palaeontologists are limited to the shells. The incorporation of microstructural data *s.l.* in the diagnoses could be of great help to improve the taxonomy of fossils and the phylogeny of Molluscs.

Acknowledgement

References

Abolins-Krogis, A. (1958) The morphological and chemical characteristics of organic crystals in the regenerating shell of *Helix pomatia*. *Acta Zool.* **39**, 19–38.

Al-Bassam, K.S. (2005) Strontium content and Na/Ca ratio in recent mollusk shells as salinity indicators in fluvial water systems. *Iraqi Bull. Geol. Min.* **1**, 21–33.

Balogh, K.V. (1988) Heavy metal pollution from a point source demonstrated by mussel (Unio pictorum L.) at lake Balaton, Hungary. *Bull. Environ. Contam. Toxicol.* **41**, 910–914.

Bevelander, G. (1952) Calcification in Molluscs. III. Intake and deposition of Ca^{45} and P^{32} in relation to shell formation. *Bio. Bull.* **102**, 9–15.

Bogan, A.E. & Roe, K. (2008) Freshwater bivalve (Unioniformes) diversity, systematics, and evolution: status and future directions. *J. North Am. Bentholog. Soc.* **27**, 349–369.

Boggild, O.B. (1930) The shell structure of the molluscs. Kongelige *Danske Videnskabernes Selskab, Naturvidenskabelig og mathematisk afdeling Ser. 9*, **2**, 231–326.

Bordas, J.E., Wheeler, A.P. & Sikes, C.S. (1991) Molluscan shell matrix phosphoproteins: correlation of degree of phosphorylation to shell mineral microstructure and to *in vitro* regulation of mineralization. *J. Exp. Zool.* **258**, 1–13.

Brandes, J.A., Ingall, E. & Paterson, D. (2007) Characterization of minerals and organic phosphorus species in marine sediments using soft X-ray fluorescence spectromicroscopy. *Mar. Chem.* **103**, 250–265.

Cassini, A., Tallandini, L., Favero, N. & Albergoni, V. (1986) Cadmium bioaccumulation studies in the freshwater molluscs *Anodonta cygnea* and *Unio elongatus. Comp. Biochem. Physiol.* **84C**, 35–41.

Checa, A.G. & Rodriguez-Navarro, A. (2001) Geometrical and crystallographic constraints determine the self-organization of shell microstructures in Unionidae (Bivalvia: Mollusca). *Proc. R. Soc. Lond. B: Biol. Sci.* **268**, 771–778.

Checa, A.G., Salas, C., Harper, E.M. & DE Bueno-Perez, J. (2014) Early stage biomineralization in the periostracum of the 'living fossil' bivalve *Neotrigonia. PloS ONE* **9**, 2, e90033. https://doi.org/10.1371/journal.pone.009003

Clarke, F.W. & Wheeler, W.C. (1922) The inorganic constituents of marine invertebrates. *US Gov. Prin. Off.* **124**, 1–62.

Crenshaw, M.A. & Ristedt, H. (1976) The histochemical localization of reactive groups in septal nacre from *Nautilus pompilus* L. *The Mechanism*

of Mineralization in the Invertebrates and Plants (ed. by N. Watabe & K.M. Wilbur), pp. 355–367. University of South Carolina Press, USA.

Cuif, J.P., Burghammer, M., Chamard, V., Dauphin, Y., Godard, P., Le Moullac, G., Nehrke, G. & Perez-Huerta, A. (2014) Evidence of a biological control over origin, growth and end of the calcite prisms in the shells of *Pinctada margaritifera* (Pelecypod, Pterioidea). *Minerals* **4**, 815–834.

Cuif, J.P., Dauphin, Y., Doucet, J., Salomé, M. & Susini, J. (2003) XANES mapping of organic sulfate in three scleractinian coral skeletons. *Geochim. Cosmochim. Acta.* **67**, 75–83.

Dauphin, Y. & Denis, A. (1990) Analyse microstructurale des tests de Mollusques du Callovien de Lukow (Pologne) – comparaison de l'état de conservation de quelques types microstructuraux majeurs. *Revue de Paléobiologie.* **9**, 27–36.

Dauphin, Y. (1986) Microstructure *versus* mineralogical and chemical data to estimate the state of preservation of fossil shells: a belemnitid example (Cephalopoda: Coleoidea). *Revue de Paléobiologie* **7**, 1–10.

Dauphin, Y. (2003) Soluble organic matrices of the calcitic prismatic shell layers of two Pteriomorphid Bivalves – *Pinna nobilis* and *Pinctada margaritifera*. *J. Biol. Chem.* **278**, 15168–15177.

Dauphin, Y., Ball, A.D., Cotte, M., Cuif, J.P., Meibom, A., Salomé, M., Susini, J. & Willams, C.T. (2008) Structure and composition of the nacre–prisms transition in the shell of *Pinctada margaritifera* (Mollusca, Bivalvia). *Anal. Bioanal. Chem.* **390**, 1659–1669.

Dauphin, Y., Cuif, J.P., Mutvei, H. & Denis, A. (1989) Mineralogy, chemistry and ultrastructure of the external shell layer in ten species of *Haliotis* with reference to *Haliotis tuberculata* (Mollusca: Archaeogastropoda). *Bull. Geol. Inst., Univ. Uppsala,* N.S. **15**, 7–38.

Dauphin, Y., Cuif, J.P. & Salomé, M. 2014. Structure and composition of the aragonitic shell of a living fossil: *Neotrigonia* (Mollusca, Bivalvia). *Eur. J. Mineral.* **26**, 485–494.

Dauphin, Y., Cuif, J.P., Castillo-Michel, H., Chevallard, C., Farre, B. & Meibom, A. (2013) Unusual micrometric calcite–aragonite interface in the abalone shell *Haliotis* (Mollusca, Gastropoda). *Microsc. Microanal.* **20**, 276–284.

Dauphin, Y., Cuif, J.P., Cotte, M. & Salomé, M. (2012) Structure and composition of the boundary zone between aragonite crossed lamellar and calcitic prism layers in the shell of *Concholepas concholepas* (Mollusca, Gastropoda). *Invertebr. Biol.* **131**, 165–176.

Dauphin, Y., Cuif, J.P., Doucet, J., Salomé, M., Susini, J. & Williams, C.T. (2003) *In situ* mapping of growth lines in the calcitic prismatic layers of mollusc shells using X-ray absorption near-edge structure (XANES) spectroscopy at the sulphur edge. *Mar. Biol.* **142**, 299–304.

Farre, B., Brunelle, A., Laprévote, O., Cuif, J.P., Williams, C.T. & Dauphin, Y. (2011) Shell layers of the black-lip pearl oyster *Pinctada margaritifera*: matching microstructure and composition. *Comp. Biochem. Physiol.* 159B, **3**, 131–139.

Findlater, G., Shelton, A., Rolin, T. & Andrews, J. (2014) Sodium and strontium in mollusc shells: preservation, palaeosalinity and palaeotemperature of the Middle Pleistocene of eastern England. *Proc. Geol. Assoc.* **125**, 14–19.

Freer, A., Greenwood, D., Chung, P., Pannell, C.L. & Cusack, M. (2010) Aragonite prism-nacre interface in freshwater mussels *Anodonta anatina* (Linnaeus, 1758) and *Anodonta cygnea* (L. 1758). *Cryst. Growth Des.* **10**, 344–347.

Greenfield, M.E., Wilson, D.C. & Crenshaw, M.A. (1984) Ionotropic nucleation of calcium carbonate by molluscan matrix. *Am. Zool.* **24**, 925–935.

Grégoire, C. (1961) Sur la structure submicroscopique de la conchioline associée aux prismes des coquilles de mollusques. *Bull. Inst. R. Sci. Nat. Belgique.* **37**, 1–34.

Grigor'ev, D.P. (1965) *Ontogeny of minerals.* Israel Program for Scientific Translations, 250 pp.

Haugstad, G. (2012) *Atomic Force Microscopy: Understanding Basic Modes and Advanced Applications.* John Wiley and Sons, Hoboken, NJ, USA.

Hikida, Y., Suzuki, S., Togo, Y. & Shimamoto, M. (1993) The organic matrices of the nacreous layer replaced by secondary aragonite in fossil shells of *Acila divaricata* (Mollusca: Bivalvia). *Structure, Formation and Evolution of Fossil Hard Tissues* (ed. by I. Kobayashi, H. Mutvei & A. Sahni), pp. 81–87. Tokai University Press, Japan.

Horiguchi, Y. (1959) Biochemical studies on *Pteria (Pinctada) martensii* (Dunker) and *Hyriopsis Schlegelii* (V. Martens). IX- Trace components in the shells of shellfish (part 2). *Bull. Jap. Soc. Sci. Fisher.* **25**, 397–401.

Johnstone, M. (2008) Characterization of soluble matrix from molluscan shell with an emphasis on two major phosphoproteins from the Eastern oyster, *Crassostrea virginica*. PhD Thesis, All Dissertations, Paper 222, Clemson University, USA.

Krolak, E. & Zdanowski, B. (2007) Phosphorus and calcium in the mussels *Sinanodonta woodiana* (Lea) and *Dreissena polymorpha* (Pall.) in the Konin lakes. *Arch. Pol. Fisher.* **15**, 287–294.

Kurunczi, S., Török, S. & Chevallier, P. (2001) A micro-XRF study of the element distribution on the growth front of mussel shell (Species of *Unio Crassus* Retzius). *Mikrochim. Acta.* **137**, 41–48.

Marie, B., Luquet, G., Bedouet, L., Milet, C., Guichard, N., Medakovic, D. & Marin, F. (2008) Nacre calcification in the freshwater mussel *Unio pictorum*: carbonic anhydrase activity and purification of a 95 kDa calcium binding glycoprotein. *ChemBioChem.* **9**, 2515–2523.

Marie, B., Luquet, G., Pais de Barros, J.P., Guichard, N., Morel, S., Alcaraz, G., Bollache, L. & Marin, F. (2007) The shell matrix of the freshwater mussel *Unio pictorum* (Paleoheterodonta, Unionoida). *FEBS J.* **274**, 2933–2945.

Marie, B., Zanella-Cléon, I., Le Roy, N., Becchi, M., Luquet, G. & Marin, F. (2010) Proteomic analysis of the acid-soluble nacre matrix of the Bivalve *Unio pictorum*: detection of novel carbonic anhydrase and putative protease inhibitor proteins. *ChemBioChem.* **11**, 2138–2147.

McClintock, C. (1967) Shell structure of patelloid and bellerophontoid gastropods (Mollusca). *Bull. Peabody Mus. Nat. Hist., Yale Univ.* **22**, 1–140.

Masuda, F. & Hirano, M. (1980) Chemical composition of some modern marine pelecypod shells. *Sci. Rep. Inst. Geosci. Univ. Tsukuba B.* **1**, 163–177.

Mittal, V. & Matsko, N.B. (2012) *Analytical Imaging Techniques for Soft Matter Characterization.* Springer Science and Business Media, New York.

Mutvei, H. (1977) The nacreous layer in *Mytilus, Nucula,* and *Unio* (Bivalvia). Crystalline composition and nucleation of nacreous tablets. *Calcif. Tissue Res.* **24**, 11–18.

Mutvei, H., Dauphin, Y. & Cuif, J.P. (1985) Observations sur l'organisation de la couche externe du test des *Haliotis*: un cas exceptionnel de variabilité minéralogique et microstructurale. *Bull. Mus. Natl. Hist. Nat.,* Paris, 4è sér., 7, sect. A, **1**, 73–91.

Naganuma, T., Hoshino, W., Shikanai, Y. *et al.* (2014) Novel matrix proteins of *Pteria penguin* pearl oyster shell nacre homologous to the jacalin-related prism fold lectins. *PLoS ONE* **9**(11), e112326, https://doi.org/10.1371/journal.pone.0112326

Nudelman, F., Gotliv, B.A., Addadi, L. & Weiner, S. (2006) Mollusk shell formation: mapping the distribution of organic matrix components

underlying a single aragonitic tablet in nacre. *J. Struct. Biol.* **153**, 176–187.

Ramos Silva, P., Benhamada, S., Le Roy, N. *et al.* (2012) Novel molluscan biomineralization proteins retrieved from proteomics: a case study with Upsalin. *ChemBioChem.* **13**, 1067–1078.

Ravera, O., Beone, G.M., Roberto Cenci, R. & Lodigiani, P. (2003) Metal concentrations in *Unio pictorum mancus* (Mollusca, Lamellibranchia) from of 12 Northern Italian lakes in relation to their trophic level. *J. Limnol.* **62**, 121–138.

Ravera, O., Beone, G.M., Trincherini, P.R. & RiccardI, N. (2007) Seasonal variations in metal content of two *Unio pictorum mancus* (Mollusca, Unionidae) populations from two lakes of different trophic state. *J. Limnol.* **66**, 28–39.

Rusenko, K.W. (1988) Studies on the structure and function of shell matrix proteins from the American oyster, *Crassostrea virginica*. PhD Dissertation, Clemson University, Clemson, South Carolina.

Sarashina, I. & Endo, K. (2001) The complete primary structure of molluscan shell protein 1 (MSP-1), an acidic glycoprotein in the shell matrix of the scallop *Patinopecten yessoensis*. *Marine Biotech.* **3**, 362–369.

Schoeppler, V. & Zlotnikov, I. (2017) A common growth mechanism forms the nacro-prismatic shell of *U. pictorum*. BiominXIV, Tsukuba 9–13 Oct., 149.

Schmidt, W.J. (1924) Die Bausteine des Tierkörpers in polarisiertem Lichte. F. Cohen, Bonn, 528 p.

Schöll-Barna, G., Demény, A., Serlegi, G., Fabian, S., Sümegi, P., Forizs, I. & Bajnoczi, B. (2012) Climatic variability in the Late Copper Age: stable isotope fluctuation of prehistoric *Unio pictorum* (Unionidae) shells from Lake Balaton (Hungary). *J. Paleolimnol.* **47**, 87–100.

Sikes, C.S. & Wheeler, A.P. (1983) A systematic approach to some fundamental questions of carbonate calcification. *Biomineralization and Biological Metal Accumulation* (ed. by P. Westbroek & E.W. de Jong), pp. 285–289. Springer, the Netherlands.

Simkiss, K. (1965) The organic matrix of the oyster shell. *Comp Biochem. Physiol.* **16**, 427–435.

Simkiss, K. (1976) Intracellular and extracellular routes in biomineralization. *Symp. Soc. Exp. Biol.* **30**, 423–444.

Solé, V.A., Papillon, E., Cotte, M., Walter, P. & Susini, J. (2007) A multiplatform code for the analysis of energy-dispersive X-ray fluorescence spectra. *Spectrochim. Acta.* B62, 63–68.

Taylor, J.D., Kennedy, W.J. & Hall, A. (1969) The shell structure and mineralogy of the Bivalvia. Introduction. Nuculacae – Trigonacae. *Bull. Brit. Mus. Nat. Hist., Zool.* **3**, 1–125.

U.S. Fish and Wildlife Service (2003) Species information: threatened and endangered animals and plants (On-line). Accessed August 13, 2003 at http://endangered.fws.gov/wildlife.html#Species.

Versteegh, E.A.A., Troelstra, S.R., Vonhof, H.B. & Kroon, D. (2009) Oxygen isotope composition of bivalve seasonal growth increments and ambient water in the rivers Rhine and Meuse. *Palaios* **24**, 497–504.

Versteegh, E.A.A., Vonhof, H.B., Troelstra, S.R., Kaandorp, R.J.G. & Kroon, D. (2010) Seasonally resolved growth of freshwater bivalves determined by oxygen and carbon isotope shell chemistry. *Geochem. Geophys. Geosyst.* **11**, 8. https://doi.org/10.1029/2009GC002961.

Vinogradov, A.P. (1953) The elementary chemical composition of marine organisms. *New Haven, Sears Foundation for Marine Research*, Yale University. Translated from Russian by J. Efron and J.K. Setlow, 647 p., 327 tables.

Wada, K. & Furuhashi, T. (1970) Studies on the mineralization of the calcified tissue in molluscs – XVII. Acid polysaccharide in the shell of *Hyriopsis schlegeli*. *Bull. Jap. Soc. Sci. Fisher.* **36**, 1122–1126.

Wada, K. (1956) Electron-microscopic observations on the shell structure of pearl oyster (*Pinctada martensii*). Observations of the calcite crystals in prismatic layers. *Bull. Nat. Pearl Res. Lab.* **1**, 1–6.

Wada, K. (1964) Studies on the mineralization of the calcified tissue in molluscs. X. Histochemical determination of the nature of acid mucopolysaccharide in organic crystals. *Bull. Jap. Soc. Sci. Fisher.* **4**, 993–998.

Watabe, N. & Wada, K. (1956) On the shell structure of the Japanese pearl oyster, *Pinctada martensii* (Dunker). (I) Prismatic layer. *J. Fac. Fisher., Prefect. Univ. Mie* **2**, 227–232.

Watters, G.T. (2001) The evolution of the Unionacea in North America, and its implications for the worldwide fauna. *Ecology and Evolution of the Freshwater Mussels Unionoida* (ed. by G. Bauer & K. Wächtler), pp. 281–307. Springer, Berlin.

Wheeler, A.P. (1992) Phosphoproteins of Oyster (*Crassostrea virginica*) shell organic matrix. *Hard Tissue Mineralization and Demineralization* (ed. by S. Suga & N. Watabe), pp. 171–187. Springer-Verlag, Tokyo.

Wise, S.W. (1970) Microarchitecture and mode of formation of nacre (Mother-of-Pearl) in pelecypods, gastropods, and cephalopods. *Eclogae Geol. Helv.* **63**, 775–797.

Supporting Information

Additional Supporting information may be found in the online version of this article at the publisher's website:

Fig. S1. Distribution maps (EDS) showing the absence of an organic layer between nacre and prisms, and a faint interprismatic membrane (dotted line) in two shells (A–E and F–J).

Fig. S2. XRF spectrum averaged over the XRF maps. Elemental peaks deconvolution performed using PyMCA (Solé *et al.*, 2007).